Journal of Medicinal Chemistry Article

J. Med. Chem. **2009,** *52,* 4911–4922 **4911**
DOI: 10.1021/jm900565c

The Glutamate Receptor GluR5 Agonist (*S*)-2-Amino-3-(3-hydroxy-7,8-dihydro-6*H*-cyclohepta[*d*]isoxazol-4-yl)propionic Acid and the 8-Methyl Analogue: Synthesis, Molecular Pharmacology, and Biostructural Characterization[†]

Rasmus P. Clausen,*[,‡] Peter Naur,[‡] Anders S. Kristensen,[‡] Jeremy R. Greenwood,[‡] Mette Strange,[‡] Hans Brauner-Osborne,[‡] Anders A. Jensen,[‡] Anne Sophie T. Nielsen,[‡] Ulla Geneser,[‡] Lone M. Ringgaard,[‡] Birgitte Nielsen,[‡] Darryl S. Pickering,[§] Lotte Brehm,[‡] Michael Gajhede,[‡] Povl Krogsgaard-Larsen,[‡] and Jette S. Kastrup[‡]

[‡]*Department of Medicinal Chemistry and* [§]*Department of Pharmacology and Pharmacotherapy, Faculty of Pharmaceutical Sciences, University of Copenhagen, 2 Universitetsparken, DK-2100 Copenhagen, Denmark*

Received May 3, 2009

The design, synthesis, and pharmacological characterization of a highly potent and selective glutamate GluR5 agonist is reported. (*S*)-2-Amino-3-((*RS*)-3-hydroxy-8-methyl-7,8-dihydro-6*H*-cyclohepta-[*d*]isoxazol-4-yl)propionic acid (**5**) is the 8-methyl analogue of (*S*)-2-amino-3-(3-hydroxy-7,8-dihydro-6*H*-cyclohepta[*d*]isoxazol-4-yl)propionic acid ((*S*)-4-AHCP, **4**). Compound **5** displays an improved selectivity profile compared to **4**. A versatile stereoselective synthetic route for this class of compounds is presented along with the characterization of the binding affinity of **5** to ionotropic glutamate receptors (iGluRs). Functional characterization of **5** at cloned iGluRs using a calcium imaging assay and voltage-clamp recordings show a different activation of GluR5 compared to (*S*)-glutamic acid (Glu), kainic acid (KA, **1**), and (*S*)-2-amino-3-(3-hydroxy-5-*tert*-butyl-4-isoxazolyl)propionic acid ((*S*)-ATPA, **3**) as previously demonstrated for **4**. An X-ray crystallographic analysis of **4** and computational analyses of **4** and **5** bound to the GluR5 agonist binding domain (ABD) are presented, including a watermap analysis, which suggests that water molecules in the agonist binding site are important selectivity determinants.

Introduction

Glutamic acid (Glu[a]) is the primary central excitatory neurotransmitter in the brain and plays a key role in normal functions of the central nervous system (CNS) but also in a number of CNS disorders.[1−4] Upon synaptic release, Glu activates a highly heterogeneous group of receptors comprising both the G-protein coupled metabotropic Glu receptors (mGluRs) as well as the ionotropic Glu receptors (iGluRs) that are ligand-gated ion channels.[1,5] On the basis of structural, functional, and pharmacological characteristics, iGluRs are categorized into three classes according to selective activation by the agonists *N*-methyl-D-aspartic acid (NMDA), (*S*)-2-amino-3-(3-hydroxy-5-methylisoxazol-4-yl)propionic acid ((*S*)-AMPA, **2**), and kainic acid (KA, **1**) (Figure 1). The iGluRs are homo- or heteromeric assemblies of subunits forming ion channels, AMPA receptors being made up of the GluR1−4 subunits, NMDA receptors of NR1, NR2A-D, and NR3A-B, and KA receptors of GluR5−7 and KA1−2 subunits.[1,6−8] In recent years, X-ray crystallographic studies of a soluble construct (GluR2-S1S2) of the agonist binding domain (ABD) of GluR2 containing various AMPA receptor ligands have provided structural information about ligand recognition as well as activation and desensitization mechanisms.[9−11] Recently, ABDs of NR1, NR2A, NR3A-B, GluR3-GluR6, and the δ2 receptor have appeared.[12−21] The ABD has a clamshell-like structure that closes upon ligand binding. This motion probably leads to opening of the ion channel. It has been observed that the degree of domain closure induced by ligands in GluR2 correlates with the relative agonist efficacy of ligands measured by the magnitude of the induced ion current.[22,23] These constructs crystallize as dimers, and it is now generally believed that the iGluR complexes are dimers of dimer assemblies containing a total of four ligand binding sites.

We recently reported that (*S*)-2-amino-3-(3-hydroxy-7,8-dihydro-6*H*-cyclohepta[*d*]isoxazol-4-yl)propionic acid ((*S*)-4-AHCP, **4**) is a potent and selective agonist at homomeric GluR5 receptors.[24] This finding explained the paradoxically high potency in the activation of cat spinal interneurons but relatively low affinity to known Glu binding sites previously observed.[25] The X-ray crystal structure of **4** in the GluR2-S1S2 construct was recently reported and in this structure the ABD is partially closed, which is in agreement with previous observations that **4** is a partial agonist at GluR2.[26] However, at GluR5, **4** shows superagonistic characteristics by inducing a larger current than the full agonists KA and Glu, in

[†]PDB ID: 2WKY.

*To whom correspondence should be addressed. Phone: +45 35 33 65 66. Fax: +45 35 33 60 40. E-mail: rac@farma.ku.dk.

[a] Nonstandard abbreviations: 4-AHCP, 2-amino-3-(3-hydroxy-7,8-dihydro-6*H*-cyclohepta[*d*]isoxazol-4-yl)propionic acid; iGluRs, ionotropic glutamate receptors; KA, kainic acid; ATPA, 2-amino-3-(3-hydroxy-5-*tert*-butylisoxazol-4-yl)propionic acid; ABD, agonist binding domain; Glu, (*S*)-glutamic acid; CNS, central nervous system; mGluRs, metabotropic glutamate receptors; NMDA, *N*-methyl-D-aspartic acid; AMPA, 2-amino-3-(3-hydroxy-5-methylisoxazol-4-yl)propionic acid; ConA, Concanavalin A; GluR2-S1S2, soluble construct of the agonist binding domain of GluR2; GluR5-S1S2, soluble construct of the agonist binding domain of GluR5; DFT, density functional theory.

Published on Web 07/09/2009

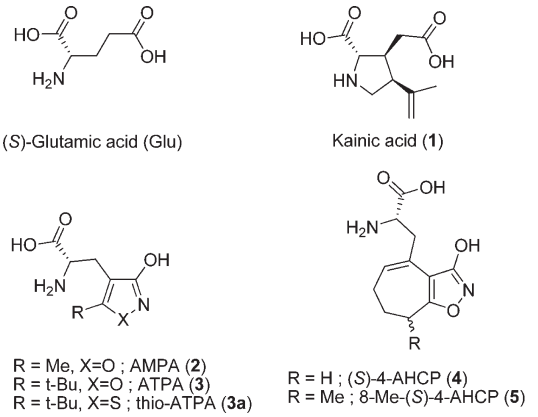

Figure 1. Structures of Glu and selective iGluR agonists **1**−**5**.

voltage-clamp measurements using *Xenopus laevis* oocytes and from measurements of intracellular calcium concentrations in HEK293 cells,[24] when these systems are expressing GluR5(*Q*) and treated with Concanavalin A (ConA) to block desensitization. Thus, **4** is an important tool for studying the functional properties of GluR5 and other KA receptor subtypes because it displays a different pharmacology compared to other GluR5 ligands.

Two synthetic routes to **4** have been reported of which one is stereoselective, but the yields are rather low. Thus, a more efficient route to **4** and analogues is desirable. Furthermore, **4** also has significant AMPA receptor activity. We here present a preparative synthetic route to **4**, and the analogue (*S*)-2-amino-3-((*RS*)-3-hydroxy-8-methyl-7,8-dihydro-6*H*-cyclohepta[*d*]isoxazol-4-yl)proionic acid (**5**) with improved pharmacological properties, together with an X-ray crystal structure of **4** in the soluble construct of the GluR5 ABD. The interactions of **4** and **5** with the AMPA and KA receptor subtypes GluR2 and GluR5, respectively, are compared using computational binding site analysis methods including the recently reported watermap analysis.

Results

Chemistry. The new synthetic route to **4** (Scheme 1) commenced like previously reported syntheses from *O*-alkyl ketone **9a**,[24,25] which was prepared from ethyl 2-oxoheptanecarboxylate **6a** in three steps via **7a** and **8a**. Similarly, the methylated analogue **9b** could be synthesized from ethyl (*RS*)-3-methyl-2-oxoheptanecarboxylate **6b**[27] via **7b** and **8b**. Treatment of ketones **9a** and **9b** with hydrazine gave the hydrazones **10a** and **10b** in 97% and 89% yield, respectively. Subsequently, treatment with iodine yielded vinyl iodides **11a** and **11b**, in 83% and 53% yield, respectively, and these iodides were substrates in Negishi couplings. Thus, the (*S*)-serine derived iodide **12** was converted to the zinc iodide **13**,[28] which was used directly in Pd-catalyzed cross-coupling reactions with vinyl iodides **11a** and **11b**, furnishing **14a** and **14b** in 38% and 55% yield, respectively. Deprotection of **14a** upon treatment with 6 M HCl in AcOH for 4 h at 120 °C yielded **4** in 89% yield with 87% ee. Similarly, compound **5** was obtained in 86% yield with 86% ee from **14b**. Recrystallizations improved the enantiomeric excess to >95%. Attempts to separate the two diasteromers of **5** were not successful by either crystallization or HPLC. In an attempt to synthesize the chain homologue of **4**, the aspartic acid derived iodide **15**[29] was converted to the zinc iodide **16** that was employed in a cross-coupling reaction with vinyl

Scheme 1[a]

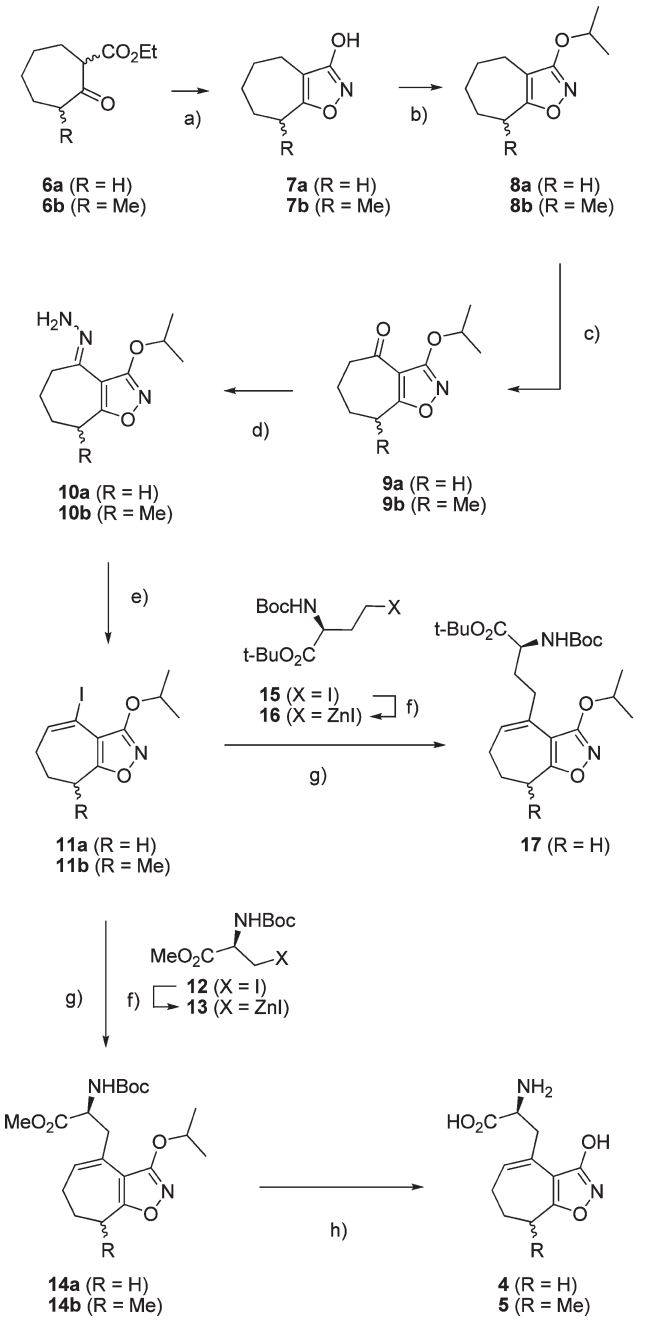

[a] Reagents: (a) NH_2OH, H_2O; (b) *i*Pr−Br, DMF, K_2CO_3; (c) $Na_2Cr_2O_7 \cdot 2H_2O$, H_2SO_4, AcOH; (d) NH_2NH_2, EtOH; (e) I_2, THF Et_3N; (f) Zn, DMF; (g) $Pd(OAc_2)$, dicyclohexyl-*m*-biphenyl phosphine; (h) 12 M aq. HCl, AcOH.

iodide **11a**, providing the protected homologue **17** in 57% yield. However, deprotection attempts under various acidic conditions yielded complex mixtures from which we were unable to isolate the desired final product.

We also investigated the possibility of making six-membered ring homologues of **4** and **5** using the same synthetic strategy (Scheme 2). Thus, ketones **21a** and **21b** were obtained in three steps from **18a** and **18b** via isoxazolols **19a** and **19b** and the *O*-alkylated **20a** and **20b**, respectively. These ketones were converted into hydrazones **22a** and **22b** in 99% and 89% yield, respectively, that upon treatment with iodine yielded vinyl iodides **23a** and **23b** in 63% and 53% yield,

respectively. The vinyl iodides **23a** and **23b** were employed in a Pd-catalyzed cross-coupling with zinc iodide **13** providing the protected ring homologues **24a** and **24b** in 52% and 55% yield, respectively. Again, deprotection of these protected amino acids under acidic conditions yielded complex mixtures and we did not obtain the desired final products.

Scheme 2[a]

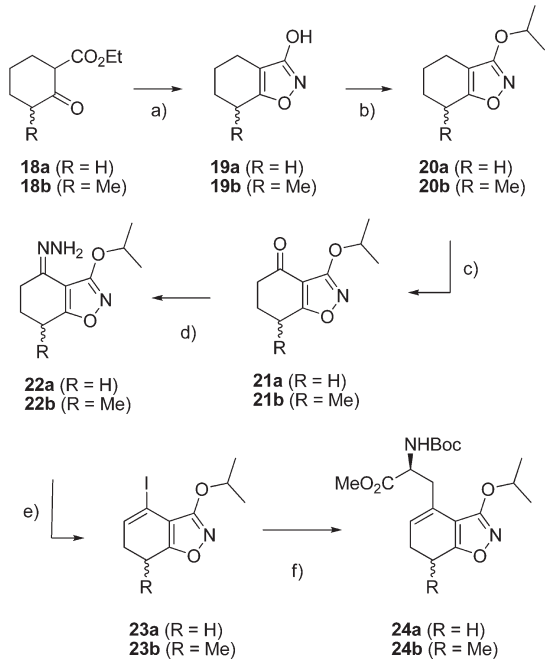

[a] Reagents: (a) (1) NH_2OH, H_2O; (b) *i*Pr−Br, DMF, K_2CO_3; (c) $Na_2Cr_2O_7 \cdot 2H_2O$, H_2SO_4, AcOH; (d) NH_2NH_2, EtOH; (e) I_2, THF Et_3N; (f) **11**, $Pd(OAc_2)$, dicyclohexyl-*m*-biphenyl phosphine.

Table 1. Binding Data on Ionotropic Glutamate Receptors in Rat Cortical Membranes[a]

compd	IC_{50} (μM) [^{3}H]AMPA	IC_{50} (μM) [^{3}H]KA	K_i (μM) [^{3}H]CGP 39653
2[b]	0.039	> 100	> 100
3[c]	1.8	23	> 100[d]
4[e]	0.28	1.6	> 100
5	9.7 [5.02 ± 0.05]	8.3 [5.09 ± 0.06]	> 100

[a] The numbers in brackets [min, max] indicate mean ± SEM according to a logarithmic distribution. [b] From ref 52. [c] From ref 53. [d] [^{3}H]CPP. [e] From ref 24.

Pharmacology. The affinity of compound **5** for native AMPA, KA, and NMDA receptors was initially determined in [^{3}H]AMPA, [^{3}H]KA, and [^{3}H]CGP 39653 competition radioligand displacement assays, respectively, using cell membranes prepared from rat cortical brain tissue (Table 1). The affinity of **5** for AMPA binding sites is more than an order of magnitude lower than that of **4** and 5-fold weaker than that of (*S*)-2-amino-3-(3-hydroxy-5-*tert*-butyl-4-isoxazolyl)propionic acid ((*S*)-ATPA, **3**). Also, the affinity of **5** for KA binding sites is reduced 5-fold compared to **4**, although it is still 3-fold more potent than **3**. The affinities of compounds **4** and **5** were further evaluated at recombinant GluR1−7 expressed as homomeric receptors in *Sf9* cells (Table 2). In this assay, compounds **4** and **5** are virtually equipotent at GluR5, but at all other subtypes, compound **5** displays approximately an order of magnitude lower affinity than compound **4**.

Compound **5** was further characterized functionally using HEK293 cell lines stably expressing homomeric GluR1−6 by measuring the increase of intracellular Ca^{2+} upon iGluR activation using Fluo-4/AM as a fluorescent Ca^{2+} indicator (Table 3).[30] In this assay, compound **5** exhibit reduced agonist potencies at GluR1−4 AMPA receptors compared to **4**, whereas the potency at iGluR5 is maintained. No response at GluR6 is observed for **4** or **5** at concentrations up to 1 mM. Thus, compound **5** more selectively activates GluR5 than **4**. As for **1** and **4**, compound **5** is a partial agonist at AMPA receptors in this assay, whereas **3** is a full agonist. As observed previously for **4**, the response induced by **5** at ConA treated GluR5 is greater than those elicited by Glu, **1**, and **3**. To further establish the functional characteristics of **5** seen in the Fluo-4/AM assay, we performed functional characterization using voltage-clamp measurements at oocytes expressing GluR1 and GluR5 (Table 4, Figure 2). Again, **5** is more selective as compared to previously reported data for **3** and **4**.[24,31]

X-ray Crystal Structure. The soluble GluR5-S1S2 construct comprising the agonist binding domain of the receptor[16] was cocrystallized with **4** in order to acquire detailed knowledge on the binding mode of **4** in GluR5 (Figure 3A). The protein crystallized in space group $P4_12_12$, with two molecules forming a dimer in the asymmetric unit and reflections extended to 2.2 Å resolution (Table 5). Investigation of the ligand-binding cavity reveals that the ligand is bound with the α-amino acid part of the molecule anchored primarily by charge−charge interactions to Arg523 and Glu738 in a manner very similar to that observed in other structures of the ABD of iGluRs and with additional hydrogen bonds to backbone as well as side chain atoms of the protein (Table 6 and Figure 3B). In the distal part of the ligand, the exocyclic oxygen and the nitrogen atom of the isoxazole ring act as a mimic of the γ-carboxylate moiety of

Table 2. Receptor Binding Affinity at Cloned Subtypes Expressed in *Sf9* Cells

	compounds					
	3		**4**		**5**	
receptor	K_i (nM) pK_i ± SEM[a]	n_H[b]	K_i (nM) pK_i ± SEM]	n_H	K_i (nM) pK_i ± SEM]	n_H
$GluR1_o$	2780 [3.526 ± 0.050]	1.10 ± 0.11	232 [2.364 ± 0.030]	1.03 ± 0.01	1550 [3.177 ± 0.077]	0.93 ± 0.04
$GluR2(R)_o$	1660 [3.213 ± 0.051]	0.81 ± 0.05	175 [2.243 ± 0.020]	0.95 ± 0.02	6310 [3.782 ± 0.091]	1.04 ± 0.10
$GluR3_o$	2040 [3.309 ± 0.014]	0.75 ± 0.03	173 [2.231 ± 0.058]	0.97 ± 0.05	1110 [3.024 ± 0.081]	0.98 ± 0.04
$GluR4_o$	2140 [3.322 ± 0.060]	0.89 ± 0.03	202 [2.295 ± 0.065]	0.90 ± 0.05	2200 [3.338 ± 0.031]	1.04 ± 0.02
GluR5(*Q*)	2.13 [0.325 ± 0.041]	0.96 ± 0.03	2.57 [0.399 ± 0.057]	0.93 ± 0.01	5.08 [0.696 ± 0.066]	0.98 ± 0.02
$GluR6(VCR)_A$	> 1000000		> 100000		> 100000	
$GluR7_A$	2530 [3.399 ± 0.045]	0.87 ± 0.08	199 [2.247 ± 0.101]	0.92 ± 0.05	1380 [3.113 ± 0.076]	1.04 ± 0.04

[a] Mean pK_i ± SEM (nM) from at least three experiments conducted in triplicate at 16 concentrations of the compound. [b] Hill coefficient, mean ± SEM.

Table 3. Functional Characterization of Glu, **1**, **3**, **4**, and **5** at Stable GluR HEK293 Cell Lines in the Fluo-4/AM Assay[a]

		compounds				
receptor		Glu[b]	**1**[b]	**3**[b]	**4**[b]	**5**
$GluR1_i$	EC_{50} (μM)	51	23	730	32	70 [4.2 ± 0.2]
	R_{max} (%)	100	18	101	28	29 ± 3
$GluR2Q_i$	EC_{50} (μM)	190	380	> 1000	92	160 [3.8 ± 0.4]
	R_{max} (%)	100	15		24	11 ± 3
$GluR3_i$	EC_{50} (μM)	52	40	630	13	48 [4.2 ± 0.04]
	R_{max} (%)	100	45	100	54	46
$GluR4_i$	EC_{50} (μM)	20	47	150	6.7	35 [3.8 ± 0.4]
	R_{max} (%)	100	55	102	79	68 ± 6
GluR5Q	EC_{50} (μM)	140	37	1.8	0.58	0.86 [6.1 ± 0.2]
	R_{max} (%)	100	97	114	147	147 ± 8
GluR6Q	EC_{50} (μM)	73	1.8	> 1000	> 1000	> 1000
	R_{max} (%)	100	98			

[a] EC_{50} values and maximal response values (R_{max} as % of R_{max} of Glu) are given. For compound **5**, pEC_{50} ± SEM values in brackets are given. [b] From Strange et al.[30]

Table 4. Potencies from Functional Characterization of **3**, **4**, and **5** Using Two-Electrode Voltage Clamp Recordings on *Xenopus laevis* Oocytes Expressing Cloned GluR Subtypes

	compounds			
	3	**4**	**5**	
receptor	EC_{50} (μM)	EC_{50} (μM)	EC_{50} (μM)	n_{Hill}
GluR5(*Q*)	0.66[31]	0.13[24]	0.24 [6.6 ± 0.8]	1.29 ± 0.12
GluR1	62[31]	4.5[24]	70 [4.2 ± 0.3]	0.91 ± 0.13
NR1/NR2A	ND	ND	> 1000	ND

Glu when compared to the structure of GluR5-S1S2 complexed with Glu (Figure 3C).[16] Introduction of the seven-membered ring has two consequences: (1) Four water molecules (W3, W5, W6, and W7, Figure 3C) participating in a hydrogen-bond network between the protein and the endogenous ligand Glu are displaced by the ring, which thereby almost entirely fills this subcavity of the protein. (2) The ring acts as a spacer that keeps the ABD in a partially open conformation (9−11° more open as compared to GluR5 in complex with Glu, PDB code 1YCJ[16]).

In the structure of GluR2-S1S2 in complex with **4**, the ligand was found in two conformations caused by a ring flip in the seven-membered ring (Figure 3D).[26] In the GluR5-S1S2 structure, the majority of the electron density can be explained by a single conformation of **4**.

Molecular Modeling. Docking and Design. When **4** was first docked to GluR2 and a homology model of GluR5[24] and compared with the GluR5-selective ligand (*S*)-2-amino-3-(5-*tert*-butyl-3-hydroxyisothiazol-4-yl)propionic acid (**3a**) (PDB: 2AIX), docking scores and structural analysis indicated that GluR5 probably accommodates a methyl substituent at position 8 better than GluR2. In particular, Ser721 and Ser741 in GluR5 (Thr686 and Met708 in GluR2) were hypothesized to provide extra space for or clash with the substituent, respectively. Solving the experimental structures of **4** in complex with GluR2-S1S2 (PDB: 1WVJ)[26] and GluR5-S1S2 (PDB: YYYY; present study) supports this idea, and accordingly, analogue **5** was synthesized, expecting that introduction of a methyl group at position 8 would increase potency at GluR5 and decrease potency at GluR2, thus improving GluR5 versus GluR2 selectivity.

Conformational Preferences of 4 and 5. In principle, the seven-membered rings of **4** and of the diastereomers (2*S*,8*R*)-**5** and (2*S*,8*S*)-**5** can assume four puckering modes, depending on whether the carbon atom in position 7 is in or out of the isoxazole plane and whether position 6 is located above or below

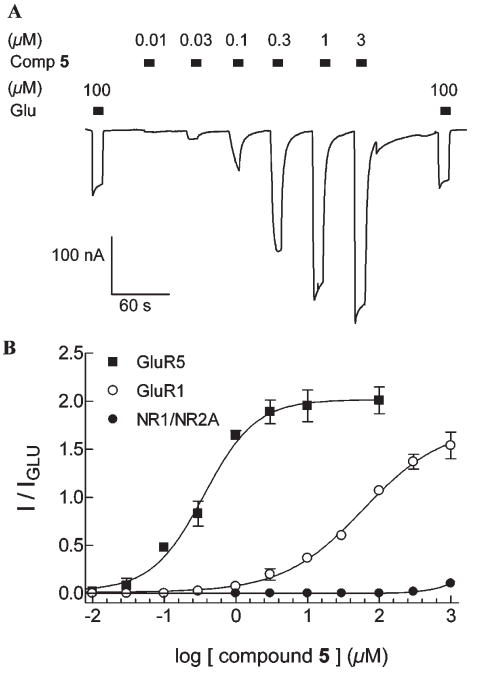

Figure 2. (A) Representative recording of currents evoked by **5** and Glu obtained from a *Xenopus laevis* oocyte expressing ConA-treated homomeric GluR5 using a two-electrode voltage clamp. (B) Concentration−response curves of **5** at homomeric GluR5 (■), homomeric $GluR1_i$ (●), NR1/NR2A (○). Responses are normalized to the response evoked by a saturating concentration of Glu (100 μM). Each data point represent averaged responses from at least five different oocytes. Error bars are SEM recordings from NR1/NR2A expressing oocytes were performed in the presence of 100 μM glycine.

the plane of the ring system (that is, on the same side of or opposite to the α-amino acid side chain). Density functional theory (DFT) and ab initio calculations in water indicate that for **4**, two of these conformations are more favorable: those with the position 6 carbon atom opposite to the side chain. The same two conformations were observed in the structure of GluR2-S1S2:**4** (PDB: 1WVJ).[26] The conformation observed in GluR5-S1S2 is 1.0 (DFT) or 0.4 kcal/mol (ab initio) higher in energy than the global minimum. Examination in GluR5 of the electron density around the seven-membered ring, with re-refinement using alternative conformations, suggests that the bound structure is mostly in this higher-energy conformation,

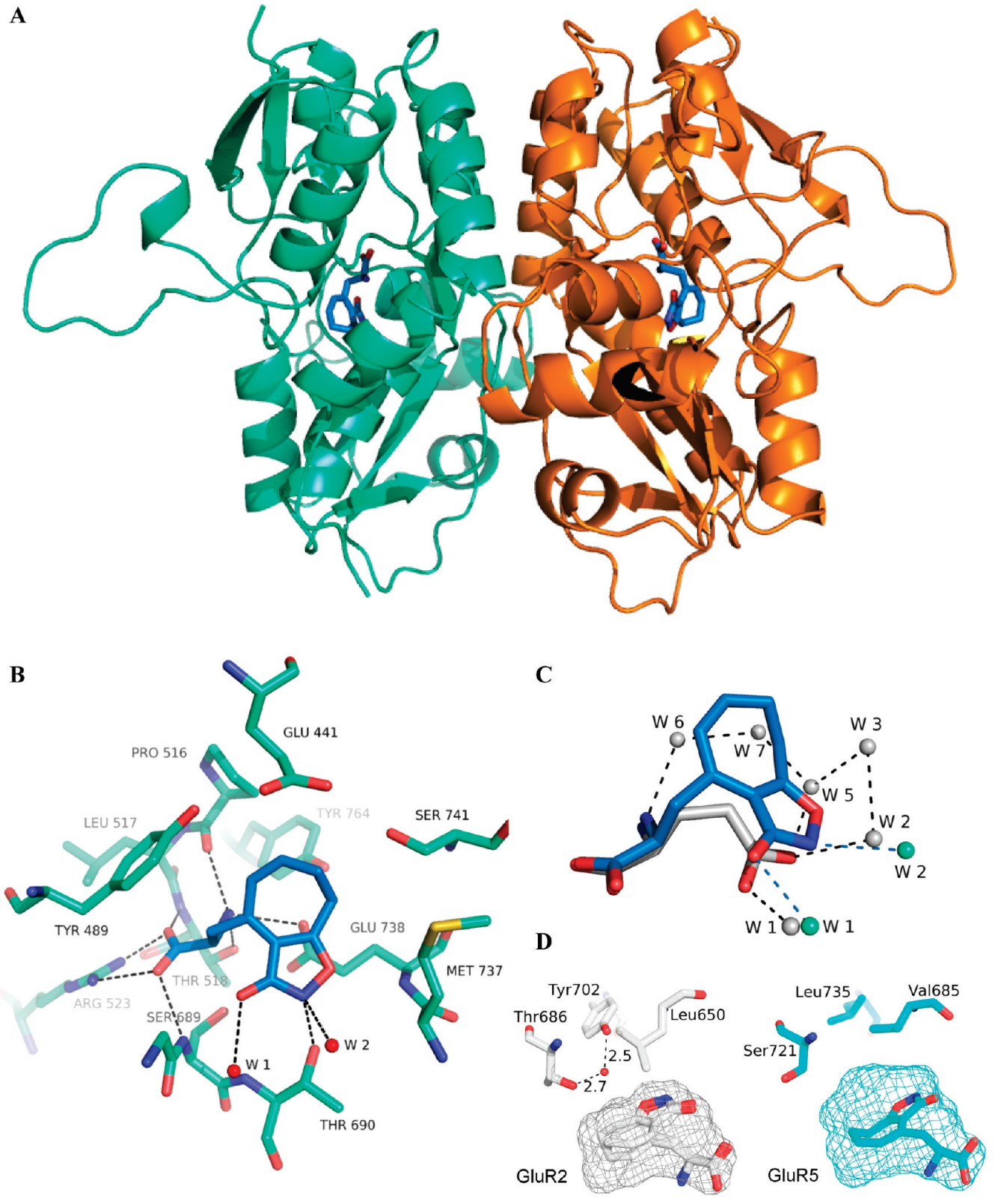

Figure 3. Structure of **4** bound to the agonist binding domain of GluR5. (A) A 2-fold symmetric dimer of GluR5-S1S2 is present in the asymmetric unit of the crystal (molA is shown in green and molB in orange). **4** is displayed in blue. (B) Close-up view of the ligand binding site (molA), including potential hydrogen bonds within 3.2 Å (dashed lines). Bonds of protein and ligand are shown in green and blue, respectively. Oxygen atoms are colored red, nitrogen atoms blue, and sulfur atoms yellow. Water molecules are shown as red spheres. (C) Superposition (on all residues) of the structures of **4** and Glu (molA, PDB: 1YCJ) in complex with GluR5-S1S2, respectively. The protein residues have been left out for clarity. **4** and water molecules are colored as in (B). In the GluR5-S1S2:Glu complex, the ligand and water molecules are colored gray. Potential hydrogen bonds from ligands to water molecules are shown. (D) Visualization of the ligand binding cavity of GluR2 and GluR5 with **4** bound. The cavity was computed using the program PASS with water molecules treated as part of the protein. Side chains of amino acids differing between GluR2 and GluR5 are shown.

Table 5. Data Collection and Refinement Statistics for GluR5-S1S2:4

space group	$P4_12_12$
unit cell (Å)	a = b = 71.3, c = 234.6
no. per a.u.[a]	2
crystal mosaicity (deg)	0.33
resolution (Å)	30−2.20
total observations	386202
unique observations	31679
$I/\sigma(I)$[b]	12.6 (2.6)
completeness (%)[b]	99.4 (99.3)
R_{sym} (%)[b,c]	9.2 (43.9)
R_{work} (%)[d]	21.1 (25.6)
R_{free} (%)[e]	24.8 (31.6)
no. protein/ligand/ion/water atoms	4042/34/2/295
average B-values protein/ligand/ion/water (Å^2)	27.1/26.4/30.9/31.6
rmsd bond lengths (Å)	0.007
rmsd bond angles (deg)	1.3
residues in allowed regions (%)[f]	97.2

[a] Number of protein molecules per asymmetric unit (a.u). [b] Values in parentheses are statistics for the highest resolution bin (2.34−2.20 Å). [c] $R_{sym}(I) = \sum_{hkl}|I_{hkl}-\langle I_{hkl}\rangle|/\sum_{hkl} I_{hkl}$, where I_{hkl} is the measured intensity of the reflections with indices hkl. [d] $R_{work} = \sum_{hkl}(||F_{o,hkl}| - |F_{c,hkl}||)/|F_{o,hkl}|$, where $|F_{o,hkl}|$ and $|F_{c,hkl}|$ are the observed and calculated structure factor amplitudes for reflection hkl. [e] Five percent of the reflections in the data set were set aside for calculation of the R_{free} value. [f] The Ramachandran plot was calculated according to Kleywegt et al.[54]

Table 6. Potential Hydrogen Bonds within 3.2 Å between GluR5-S1S2 and **4**[a]

	molA	molB
4 α carboxylate oxygen 1:		
Thr518 N	2.8	2.8
Arg523 Nη1	2.6	2.8
4 α carboxylate oxygen 2:		
Arg523 Nη2	2.8	2.8
Ser689 N	2.9	2.8
4 α-ammonium nitrogen:		
Pro516	2.8	2.6
Thr518 Oγ1	3.0	2.9
Glu738 Oε1	2.9	2.9
4 distal hydroxy group:		
W1	2.9	2.9
4 distal ring nitrogen:		
Thr690 Oγ1	2.6	2.6
W2	3.0	3.1
4 distal ring oxygen:		
Glu738 N	3.2	3.1

[a] The chemical structure of **4** is shown in Figure 1.

but some contribution from the alternative low-energy ring puckering seen in GluR2 cannot be ruled out. The reason for the slightly higher energy ring conformation with the carbon atom in position 7 out of the isoxazole plane in GluR5 is avoidance of close approach to the γ-hydroxyl group of Ser741, whereas the γ-methylene of Met708 in GluR2 is further away. For **5**, the conformational distribution is further affected by the preference of the 8-methyl substituent to rotate out of the isoxazole plane, disfavoring one of the conformations of each diastereomer and in particular the ring conformation of (2*S*,8*R*)-**5** corresponding to **4** in GluR5 is higher in energy. Two low energy conformations of (2*S*,8*R*)-**5** and (2*S*,8*S*)-**5** are presented in Figure 4.

Watermap Analysis. A watermap analysis was performed in order to establish whether selectivity can be understood in terms of the pattern and energies of water molecules in the binding pocket. Watermap is a binding site analysis tool based on inhomogeneous solvation theory, capable of describing the entropic and enthalpic contributions to the free energies of individual receptor hydration sites, by clustering the results from an explicit solvent molecular dynamics simulation.[32,33] Using the proteins only from GluR2-S1S2:**4** (PDB: 1WVJ)[26] and from GluR5-S1S2:**4** (molB), a pair of MD simulations were run and analyzed, leading to the watermaps shown in Figure 5. The agreement between the watermap sites and the experimental water and ligand heteroatom positions was generally very tight. Although there were minor differences in the networks of water molecules displaced by ligand in each receptor, **4** displaces roughly 10 water molecules in both cases and stabilizes W1 and W2, seen in the majority of iGluR agonist complexes. However, in GluR2 at the degree of domain closure induced by **4**, the ligand sequesters two high-energy water molecules: W3 (5.5 kcal/mol) and W8 (7.0 kcal/mol). In GluR5-S1S2:**4**, W3 is absent both in the watermap and in the X-ray structure, while W8, which is experimentally observed in molB, is much lower in watermap energy (0.2 kcal/mol)—two changes that are expected to confer selectivity. Furthermore, in GluR5, a new water molecule near the ligand, W9, is favorably stabilized. Ser741 and Ser721 (Met708 and Thr686 in GluR2) contribute to the stability of W8 and W9 in GluR5. Finally, in the space between Val685 and the ligand in GluR5 (but not between Leu650 and the ligand in GluR2), watermap predicts a mildly unfavorable displaceable hydration site Wx (1.2 kcal/mol), although only at partial occupancy (64%) and not experimentally observed. This suggests an opportunity for increased selectivity if Wx is displaced, as would be the case by the methyl group of (2*S*,8*R*)-**5**. In summary, the watermaps indicate that the selectivities of **4** and **5** can be understood in terms of the free energies of the binding site water molecules that differ between GluR2 and GluR5 near the ligand.

Binding Mode of 5 and Stereoselectivity. To model the binding mode of **5** and determine which diastereomer is likely to be more active, four local minimum-energy conformations of (2*S*,8*R*)-**5** and (2*S*,8*S*)-**5** with the charge-bearing heteroatoms constrained to approximate the experimental positions were least-squares superimposed with the experimental coordinates of **4**. The complexes were minimized, treating the ligand with DFT and the receptor with molecular mechanics (QM-MM). Side chains in contact with the ligand were allowed to move freely during minimization. In particular, the conformation of Met737 was found to adjust to maximize favorable contact with the ligand. Although it was not possible to determine with certainty the precise preferred ring-puckering mode of **5** when bound, Figure 4 depicts a low-energy complex for each diastereomer. In general, (2*S*,8*R*)-**5** produced lower energy complexes than (2*S*,8*S*)-**5**, indicating (2*S*,8*R*)-**5** to be a more active eutomer. Figure 4 also shows the hydrophobic and hydrophilic surfaces (shown as site maps) in the vicinity of the 8-position. These observations illustrate that above the isoxazole plane of the ligands is a more hydrophilic region with limited space. The 8-methyl group of (2*S*,8*S*)-**5** must bend away to avoid it, forcing part of the seven-membered ring downward below the preferred zone indicated by the binding mode of **4**. By contrast, the 8-methyl group of (2*S*,8*R*)-**5** can be neatly

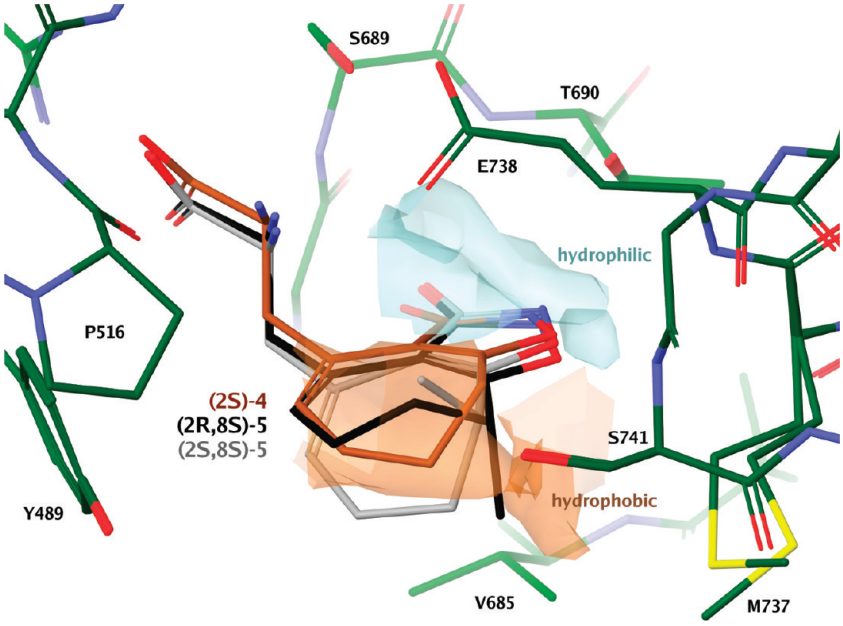

Figure 4. QM-MM minimized complexes of (2*S*,8*R*)-**5** (black) and (2*S*,8*S*)-**5** (gray) in GluR5, superimposed with **4** (brown). Hydrophobic and hydrophilic site map isopotentials near chiral position 8 are indicated in tan and cyan, respectively.

acccomodated by a hydrophobic volume below the isoxazole plane, in contact with Val685, Ser721 and Met737. The smaller volume of the corresponding hydrophobic space in GluR2 due to Thr686 and Leu650, along with the aforementioned weak hydration site Wx in GluR5, suggest that it is the (2*S*,8*R*)-**5** diastereomer that confers the observed increased GluR5 selectivity of **5** compared with **4**. Thus, these studies indicate that selectivity and potency of this class of compounds may be improved further by synthesizing (2*S*,8*R*)-**5** analogues stereoselectively. However, initial attempts to develop a synthetic route for this were not successful and the diastereomers could not be separated.

Discussion

We have presented a new stereoselective synthetic route to the specific GluR5 agonist **4** as well as the X-ray crystal structure of **4** bound to the GluR5 ABD. Furthermore, we have presented structure-based design, synthesis, and pharmacological characterization of a new analogue **5**, which turned out to be one of the most potent and selective GluR5 agonists yet described. Compound **4** is interesting because it induces an increased response at ConA-treated homomeric GluR5 receptors compared to the full agonists Glu, **3**, and **1**.[24] This is observed when GluR5 is expressed either transiently in *Xenopus laevis* oocytes or stably in HEK293 cells.[24,30] We decided to investigate the possibility of improving the synthesis of **4** and the pharmacological profile by making a new designed analogue **5**. Comparison of the X-ray structure of **4** in the GluR2 agonist binding domain construct with **4** docked in a homology model of the GluR5 agonist binding domain suggested that the selectivity could be improved by introducing increased steric bulk at the 8-position.

We focused on improving the synthetic route from **7a**, which in the first reported procedure[25] provided racemic **4** in 3% yield and in the later stereoselective route[24] led to (*S*)-**4** with a yield of 0.4%. Inspired by the use of a Negishi type cross-coupling reaction for introducing the alanine side chain by Jackson and co-workers,[28] **4** could be synthesized from **7a** in 28% yield with an enantiomeric excess of 89%. We investigated the possibility of using the synthetic strategy to obtain an alkylated analogue of **4** as well as ring and chain homologues. However, the deprotection conditions produced the desired compounds as the main product only for the 8-methylated compound **5**, whereas the other analogues yielded complex reaction mixtures in which the desired product could not be identified. A new synthetic route to ketone **7a** employing a different *O*-protecting group would be required to further improve this synthesis. Control of the stereochemistry at the 8-position of **5** would also be an objective of such a route.

A pharmacological and biostructural characterization of **4** and **5** was performed as well. The pharmacological studies conclude that **5** is more selective than **4** in two different functional assays and this selectivity profile was also seen in competition binding experiments. The selectivity of **5** as a GluR5 agonist is comparable to that of the standard GluR5 ligand **3**. Both compounds **4** and **5** induced an increased response at homomeric GluR5 receptors compared to the full agonists Glu, **1**, and **3** when the receptor is treated with ConA to block desensitizitation (Figure 2 and Table 3). These results suggest that these two compounds behave like superagonists of GluR5, inducing a larger current than glutamate at saturating concentrations when receptor densitization is inhibited by ConA. This behavior has to our best knowledge not previously been observed with any other iGluR agonist and may explain previously reported high activity of **4** observed at cat spinal interneurons.[25] The superagonist behavior cannot be readily understood at present and requires more detailed kinetic studies of GluR5 activation, and **4** and **5** will be important tools in such studies. Although these compounds behave as superagonists, the crystal structure of **4** in the GluR5 ABD displays only partial domain closure. In X-ray crystal structures of GluR2, this is observed with compounds that are partial agonists and also in the structure of the partial agonist domoic acid in GluR5-S1S2.[34] Thus, the current structure presents a challenge to the previously observed relationship between the degree of domain closure and the response induced by orthosteric ligands,[35] which has led to the

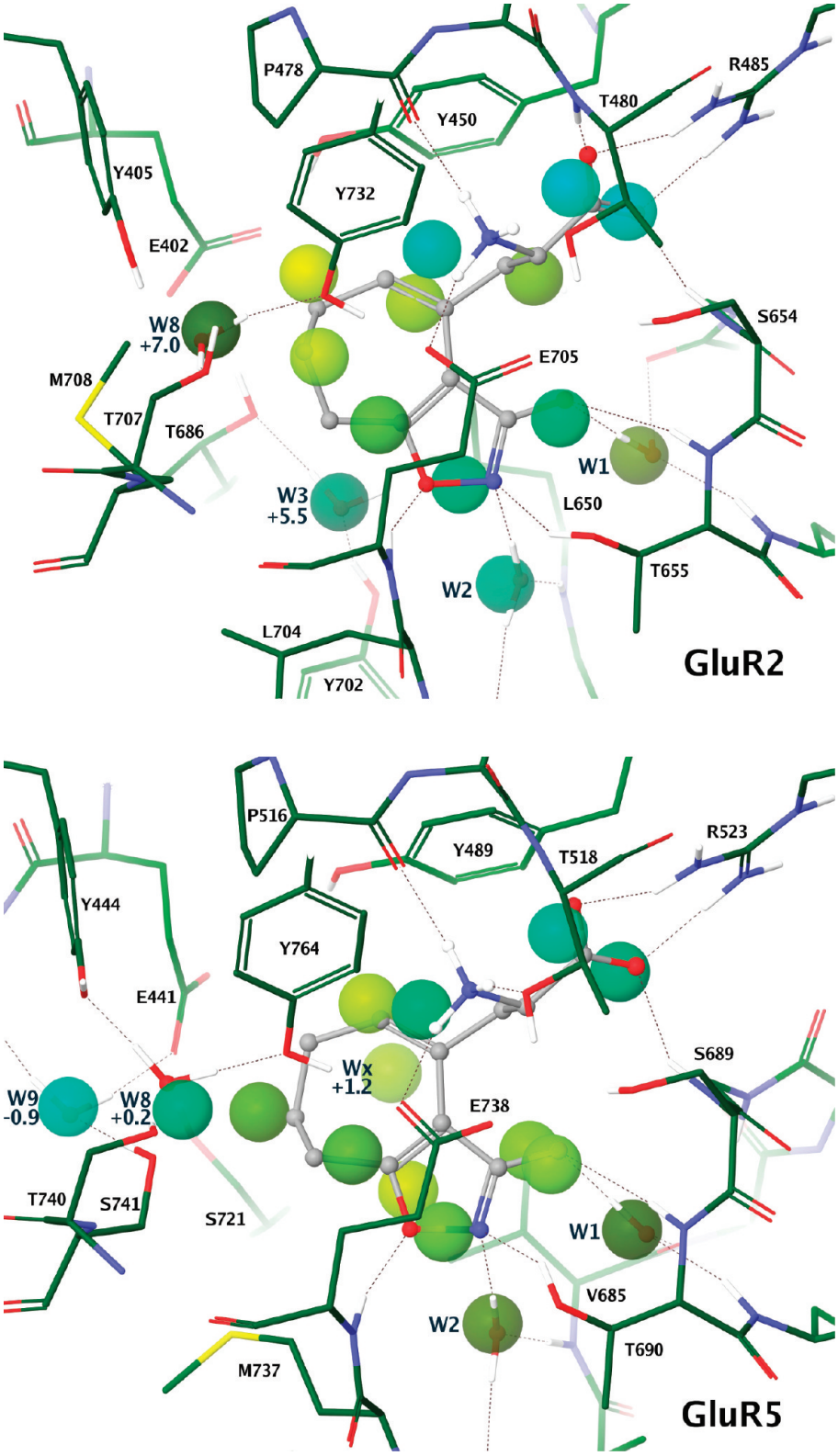

Figure 5. Watermaps of GluR2 and GluR5 from molecular dynamics, using the protein only from GluR2-S1S2J:**4** (PDB: 1WVJ) and from GluR5-S1S2:**4** (molB). Experimental ligand (gray) and water positions included for comparison (ball-and-stick) together with H-bond network (fine dashed lines). Transparent spheres indicate clustered water positions, color-coded by entropic (green) and enthalpic (cyan) contribution to free energy (darker is higher ΔG). Key water molecules nearby but not displaced by ligand are labeled W1−W3, W7−8, and Wx, together with selected ΔGs in kcal/mol. Ligand-stabilized water molecules W1 and W2 are observed in both GluR2 and GluR5. High energy water W3 in GluR2 is not predicted or observed in GluR5. W8 is greatly stabilized in GluR5 vs GluR2. Low energy water W9 in GluR5 is not predicted or observed in GluR2. Low occupancy hydration site Wx (64%) is predicted but too diffuse for observation in GluR5 and absent in GluR2.

hypothesis that agonist efficacy is positively correlated to a high degree of domain closure in kainate receptors. However, a possible explanation for the observed discrepancy could also be that the use of ConA in our functional assays does not

completely inhibit GluR5 desensitization and that **4** and **5** desensitizes GluR5 to a lesser extent than glutamate.

GluR5-S1S2 in complex with **4** shows many similar binding features to the GluR2 structure but also some key differences in the binding pocket in particular with respect to the pattern of waters. We therefore performed a watermap analysis of the GluR5 agonist binding site in comparison with GluR2 to understand the role of individual water molecule binding sites, both observed and virtual, in the selectivity observed. This analysis disclosed that the increased activity of **4** and **5** at GluR5 compared to GluR2 is clearly linked to changes in the energy of particular water molecules in the binding pocket that are stabilized, sequestered, or displaced by the ligand, affirming the utility of this kind of analysis. The high potency and selectivity most likely resides with the (2*S*,8*R*) diastereomer of **5** according to binding site mapping and QM-MM calculations.

In conclusion, compound **5** is one of the most potent and selective GluR5 agonists yet known and could be an important tool for further studying the functional characteristics of GluR5 in particular with respect to the increased response as well as the general physiological role of GluR5 receptors.

Experimental Section

Chemistry. General Procedures. Analytical thin-layer chromatography (TLC) was performed on silica gel F_{254} plates (Merck). All compounds were detected using UV light and/or by spraying with diluted solutions of $KMnO_4$ or $H_2SO_4/Ce(SO_4)_2$/ammonium molybdate. Ketones, 3-isoxazolols, and amino groups were developed using standard spraying solutions of 2,4-dinitrophenylhydrazine, $FeCl_3$, and ninhydrin, respectively. Column chromatography (CC) was performed on silica gel Matrex LC 60A (0.070−0.200 mm). Unless otherwise stated, the petroleum ether used for CC and recrystallizations had distillation ranges 80−100 °C and 40−60 °C, respectively. Organic phases were dried using $MgSO_4$. Melting points were determined in capillary tubes and are uncorrected. ^{1}H (300 MHz), ^{13}C (75 MHz), and associated proton test (APT) NMR spectra were recorded on a Varian Gemini-2000 BB spectrometer. Unless otherwise stated, $CDCl_3$ was used as solvent. Chemical shifts are given in ppm (δ) using TMS [^{1}H NMR (δ 0.0)] or the $CDCl_3$ peak [^{13}C NMR (δ 77.00)] as internal standards. For NMR spectra recorded in D_2O, 1,4-dioxane [^{1}H NMR (δ 3.70) and ^{13}C NMR (δ 69.48)] was used as an internal standard. Elemental analyses were performed at Analytical Research Department, H. Lundbeck A/S, Denmark, or by J. Theiner, Microanalytical Laboratory, Department of Physical Chemistry, University of Vienna, Austria, and are within ±0.4% of the theoretical values unless otherwise stated. Stereochemical purity, expressed as enantiomeric excess (ee), was determined using a Chirobiotic T column (4.6 mm × 150 mm, ASTEC) equipped with a Chirobiotic T guard column (4.6 mm × 50 mm, ASTEC). The column was eluted at 0.5 mL/min with an aqueous solution of ammonium acetate buffer (15 mM; adjusted to pH 4.0 using AcOH) and EtOH (40/60; v/v %). A TSP system consisting of a P2000 pump, an AS3000 autoinjector, and an SM5000 PDA detector was used. The % ee values were determined from peak areas at 210 nm.

(*RS*)-8-Methyl-5,6,7,8-tetrahydro-4*H*-cyclohepta[*d*]isoxazol-3-ol (7b). A solution of ethyl 3-methyl-2-oxoheptanecarboxylate (**6b**)[27] (2.07 g, 10.4 mmol) in MeOH (2 mL) was carefully added to NaOH (437 mg, 10.9 mmol) dissolved in MeOH (7 mL) and H_2O (0.5 mL) at −70 °C. To this solution was added a mixture of $NH_2OH \cdot HCl$ (1.45 g, 21 mmol) and NaOH (0.87 g, 22 mmol) in MeOH (8 mL) and H_2O (1 mL) filtered and precooled to −70 °C. The reaction mixture was allowed to warm to 0 °C over a period of 2 h. Upon addition of acetone (1 mL) the reaction mixture was added to a heated (85 °C) solution of 12 M HCl (2.5 mL). The resulting reaction mixture was refluxed for 1.5 h, reduced in vacuo, and added H_2O (50 mL). Extraction with AcOEt (3 × 50 mL), drying, filtration, evaporation, and CC (toluene−AcOEt (4:1) and 1% AcOH) gave **7b** (1.43 g, 82%), which was sufficiently pure to take further. A small sample was recrystallized (toluene−petroleum ether): mp 125.5 −126.5 °C. ^{1}H NMR δ 1.28 (3H, d, J = 7.2 Hz), 1.88−1.46 (5H, m), 1.96 (1H, m), 2.33 (1H, ddd, J = 3.5, 8.0, and 15.9 Hz), 2.44 (1H, ddd, J = 3.5, 7.5, and 15.9 Hz), 2.94 (1H, m), 11.56 (1H, br s). ^{13}C NMR δ 17.3, 20.7, 27.64, 27.66, 34.0, 34.3, 105.8, 169.7, 173.7. Anal. ($C_9H_{13}NO_2$) C, H, N.

(*RS*)-3-Isopropoxy-8-methyl-5,6,7,8-tetrahydro-4*H*-cyclohepta-[*d*]isoxazole (8b). Potassium carbonate (840 mg, 6.1 mmol) was added to a solution of **7b** (920 mg, 5.50 mmol) in dry DMF (15 mL), and the reaction mixture was left stirring for 30 min at 60 °C. Isopropyl bromide (775 μL, 8.26 mmol) was added, and the resulting reaction mixture was stirred overnight at 60 °C. The reaction mixture was cooled, H_2O (20 mL) was added, and the mixture was extracted with Et_2O (3 × 50 mL). The combined organic phases were dried, filtered, evaporated, and CC (toluene−AcOEt (9:1)) gave **8b** (890 mg, 77%) sufficiently pure for the next reaction. A sample was distilled in a Kugelrohr apparatus: bp 225 °C/12 mmHg. ^{1}H NMR δ 1.29 (3H, d, J = 6.9 Hz), 1.37 (6H, d, J = 6.1 Hz), 1.42−1.74 (4H, m), 1.74−1.85 (1H, m), 1.94 (1H, m), 2.31 (2H, m), 2.94 (1H, m), 4.87 (1H, heptet, J = 6.1 Hz). ^{13}C NMR δ 17.46, 20.75, 22.05, 22.07, 27.56, 27.78, 33.92, 34.30, 72.56, 105.38, 169.46, 173.27. Anal. ($C_{12}H_{19}NO_2$) C, H; N: calcd, 6.69; found, 6.09.

(*RS*)-3-Isopropoxy-8-methyl-5,6,7,8-tetrahydro-4*H*-cyclohepta-[*d*]isoxazol-4-one (9b). To a solution of **8b** (550 mg, 2.63 mmol) in AcOH (99.9%, 3 mL) and concentrated H_2SO_4 (400 mL) kept at 0−10 °C was added a solution of $Na_2Cr_2O_7 \cdot 2H_2O$ (818 mg, 2.74 mmol) in AcOH (5 mL). After stirring for 4 h at rt, the reaction mixture was neutralized with 12 M NaOH, H_2O was added (50 mL) and the mixture was extracted with Et_2O (3 × 50 mL). The combined organic phases were dried and evaporated, followed by CC (toluene−AcOEt (9:1)). First starting material was eluted (130 mg, 24%), then **9b** (180 mg, 31%) as a yellow oil. ^{1}H NMR δ 1.42, 1.43, 1.44 (3 × 3H, 3*d*, J = 7, 6, and 6 Hz), 1.58−2.60 (3H, m), 2.15 (1H, m), 2.70 (2H, m), 3.20 (1H, m), 4.94 (1H, heptet, J = 6.2 Hz). ^{13}C NMR δ 18.55, 20.28, 21.71, 32.76, 34.73, 44.77, 73.95, 108.22, 168.69, 179.79, 194.12.

(*RS*)-4-Hydrazono-3-isopropoxy-8-methyl-5,6,7,8-tetrahydro-4*H*-cyclohepta[*d*]isoxazole (10b). A solution of the ketone **9b** (175 mg, 0.78 mmol) in EtOH (10 mL) was treated with Et_3N (190 μL, 3.91 mmol) and hydrazine hydrate (1.1 mL, 7.89 mmol). The reaction mixture was heated under reflux for 3 h and left stirring overnight at rt. The solvent was evaporated and the residue dissolved in CH_2Cl_2 (20 mL). The solution was washed with H_2O (20 mL) and the aqueous phase extracted with CH_2Cl_2 (3 × 20 mL). The combined organic phases were dried and evaporated to give a (1:1) mixture of stereoisomers of **10b** (110 mg, 59%) as a solid. ^{1}H NMR δ 1.31 and 1.32 (3H, 2*d*, J = 6.9 and 7.5 Hz), 1.38−1.46 (6H, m), 1.56−1.72 (1H, m), 1.73−2.09 (3H, m), 2.50 (2H, m), 3.04 (1H, m), 4.93 and 5.01 (1H, 2 × heptet, J = 6.2 Hz). A sample was recrystallized (AcOEt−petroleum ether), giving a single stereoisomer of **10b**: mp 118.0−118.5 °C. ^{1}H NMR δ 1.31 (3H, d, J = 6.9 Hz), 1.41 (3H, d, J = 6 Hz), 1.44 (3H, d, J = 6 Hz), 1.58−1.73 (2H, m), 1.87−2.10 (2H, m), 2.50 (2H, m), 3.04 (1H, m), 4.93 (1H, heptet, J = 6.2 Hz), 5.33 (2H, s br). ^{13}C NMR δ 19.45, 21.31, 22.00, 22.05, 29.40, 32.16, 34.37, 73.62, 105.26, 142.61, 168.53, 172.73. Anal. ($C_{12}H_{19}N_3O_2$) C, H, N.

(*RS*)-4-Iodo-3-isopropoxy-8-methyl-7,8-tetrahydro-6*H*-cyclohepta[*d*]isoxazole (11b). A solution of I_2 (3.06 g, 12.1 mmol) in dry THF (20 mL) was dropwise added to a solution of hydrazone **10b** (1.15 g, 4.85 mmol) in dry THF (30 mL) and Et_3N (6.7 mL, 48.1 mmol) while keeping the temperature below 10 °C. The reaction mixture was then stirred for 30 min at rt followed by addition of H_2O (10 mL). The aqueous phase was extracted

with Et_2O (3 × 10 mL), and the combined organic phases were dried, evaporated, and subjected to CC (toluene−AcOEt (4:1)), yielding **11b** (1.26 g, 78%) as a dark oil. ^{1}H NMR δ 1.32 (3H, d, J = 6.9 Hz), 1.436 and 1.441 (2 × 3H, 2 × d, J = 6 and 6 Hz), 1.68 (1H, m), 2.05 (1H, m), 2.15 (2H, m), 3.13 (1H, hextet, J = 7.5 Hz), 4.94 (1H, heptet, J = 6.0 Hz), 6.78 (1H, t, J = 6.8 Hz). ^{13}C NMR δ 18.62, 21.96, 29.24, 33.36, 34.09, 73.82, 78.36, 105.28, 144.17, 166.96, 172.73.

Methyl (2*S*, 8*RS*)-2-[(*tert*-Butoxycarbonyl)amino]-3-(3-isopropoxy-8-methyl-7,8-dihydro-6*H* cyclohepta[*d*]isoxazol-4-yl)propionate (14b). 1,2-Dibromoethane (117 μL, 1.36 mmol) was added to a stirring suspension of Zn dust (1.80 g, 28 mmol) in dry DMF (2.5 mL). The mixture was repeatedly heated to reflux and allowed to cool to rt (×3). Trimethylsilyl chloride (35 μL, 0.28 mmol) was added to the mixture, which was stirred for further 45 min. The iodide (*R*)-**12**[28] (1.29 g, 3.92 mmol) was dissolved in dry DMF (2.5 mL) under N_2 and added to the Zn dispersion to generate **13**. The mixture was stirred at 50 °C until no starting material could be observed by TLC (ca. 45 min). The Zn dispersion was allowed to settle, and the supernatant was transferred by syringe to a mixture of the vinyl iodide **11b** (1.20 g, 3.60 mmol), $Pd(AcO)_2$ (41 mg, 0.18 mmol), and dicyclohexyl-*m*-biphenyl phosphine (200 mg, 0.57 mmol) in dry THF (2.5 mL). The remainder of the Zn dispersion was washed with dry DMF (2 × 500 μL) and transferred to the resulting reaction mixture, which was stirred overnight at rt. The mixture was filtered through celite and added H_2O (15 mL). Extraction with AcOEt (3 × 50 mL), drying, filtration, evaporation, and CC (toluene−AcOEt (6:1)) gave **14b** (1.13 g, 77%) as an oil. ^{1}H NMR δ 1.30 (1.5H, d, J = 7.5 Hz), 1.33 (1.5H, d, J = 7.5 Hz), 1.45−1.38 (15H, m), 1.52−1.68 (1H, m), 1.85−2.00 (1H, m), 2.10−2.36 (2H, m), 2.45 (0.5H, dd, J = 9 and 13 Hz), 2.70 (0.5H, dd, J = 9 and 13 Hz), 2.92 (0.5H, dd, J = 6 and 13 Hz), 3.10−3.19 (1.5H, m), 3.68 and 3.71 (3H, s), 4.26−4.35 (1H, m), 4.93−5.04 (2H, m), 5.73 (1H, t, J = 5.9 Hz). ^{13}C NMR δ 19.1, 19.4, 21.8, 25.2, 25.6, 28.2, 31.7, 31.9, 34.1, 34.6, 37.7, 37.8, 51.76, 51.83, 53.3, 53.5, 73.4, 79.4, 103.1, 103.3, 125.0, 125.2, 132.1, 154.7, 154.8, 167.6, 172.9, 173.0, 174.3, 174.4.

(2*S*, 8*RS*)-2-Amino-3-(3-hydroxy-8-methyl-7,8-dihydro-6*H*-cyclohepta[*d*]isoxazol-4-yl)propionic Acid Hydrochloride (5). Compound **14b**(1.09 g, 2.67 mmol) was dissolved in a mixture of 12 M HCl (6 mL), H_2O (3 mL) and AcOH (3 mL), and the mixture was heated at 120 °C for ca. 3 h. After evaporation and re-evaporation from H_2O (2 × 10 mL), the brownish residue was dissolved in H_2O (20 mL) and washed with CH_2Cl_2 (2 × 20 mL). The combined CH_2Cl_2 phases were extracted with H_2O. The combined H_2O phases was evaporated, giving **5** as a brownish−violet solid residue (660 mg, 86%, 89% ee), which was > 95% pure according to NMR, TLC, and HPLC. Recrystallization (2-propanol−H_2O) gave violet crystals (140 mg, 45% ee) and the mother liquor furnished after addition of ether 516 mg (95% ee) that upon recrystallization (2-propanol−H_2O−Et_2O) gave **5** (212 mg, 28%, ee 98.7%): mp > 200 °C. ^{1}H NMR (D_2O) δ 1.22 (1.5H, d, J = 7 Hz), 1.25 (1.5H, d, J = 7 Hz), 1.60 (1H, m), 1.88 (1H, m), 2.27 (2H, m), 2.78 (0.5H, dd, J = 8.0 and 14.3 Hz), 2.98−3.22 (2.5H, m), 4.07 (1H, m), 5.87 (1H, q, J = 6.1 Hz). ^{13}C NMR (D_2O) δ 20.86, 20.97, 28.28, 28.43, 32.74, 32.87, 37.06, 37.22, 38.53, 38.65, 55.53, 55.73, 105.79, 105.97, 124.54, 124.65, 138.00, 138.17, 170.90, 174.40, 179.46, 179.56. Anal. ($C_{12}H_{16}N_2O_4 \cdot HCl$) C, H, Cl, N.

In Vitro Pharmacology. Receptor Binding Assays. Affinities for native AMPA, KA, and NMDA receptors in rat cortical synaptosomes were determined using 5 nM [^{3}H]AMPA (55.5 Ci/mmol),[36] 5 nM [^{3}H]KA (58.0 Ci/mmol),[37] and 2 nM [^{3}H]CGP 39653 (K_d = 6 nM, 50.0 Ci/mmol),[38] respectively, with minor modifications as previously described.[39] Rat brain membrane preparations used in these receptor binding experiments were prepared according to a method previously described.[40]

Recombinant Receptor Binding Assays. *Sf*9 cells were cultured and infected with recombinant baculovirus of rat AMPA receptors ($GluR1_o$−4_o) or rat KA receptors (GluR5−7) and membranes prepared and used for binding as previously detailed.[41,42] The affinities of compound **5** at GluR1, GluR2(*R*), GluR3, and GluR4 (all as *flop* isoforms) were determined from competition experiments with 2−5 nM [^{3}H]AMPA, at GluR5-$(Q)_{1b}$ with 1−2 nM [^{3}H]SYM 2081, at GluR6$(V,C,R)_a$ using 5 nM [^{3}H] KA, and at GluR7a using 2−4 nM [^{3}H]SYM 2081. Italic letters in parentheses indicate the RNA-edited isoforms of the subunits used.

In Vitro cRNA Transcription. The cDNA encoding rat $GluR1_i$, rat NR1, rat NR2A, and rat GluR5−1a(*Q*) subunits inserted into the vectors pGEM-HE (GluR1 and GluR5) and pCIneo (NR1−1a and NR2A; kind gift from Dr. Kasper Hansen, Emory University) were used for preparation of capped cRNA transcripts. Capped mRNA was synthesized from 1 μg of linearized plasmid DNAs by in vitro transcription and purified using the mMESSAGE mMACHINE T7 mRNA-capping kit (Ambion, Austin, TX) according to the protocol supplied by the manufacturer. Purified cRNA was resuspended in H_2O to a concentration of 100 ng/μL and stored at −80 °C until use.

Electrophysiology. Preparation of Oocytes. Mature female *Xenopus laevis* (NASCO, CA) were anesthetized by submersion into a solution of 0.1% ethyl 3-aminobenzoate dissolved in double-distilled water with 1 g/L $CaCO_3$ and ovaries were surgically removed. The ovarian tissue was dissected and treated with 1.5 mg/mL collagenase in Ca^{2+}-free Barth's medium (in mM: 88 NaCl, 1 KCl, 15 $Ca(NO_3)_2$, 0.82 $MgSO_4$, 2.4 $NaHCO_3$, 5 HEPES, pH 7.4) for 45−90 min at room temperature. Collagenase-treated oocytes were subsequently maintained in Barth's medium supplemented with 0.41 mM $CaCl_2$. On the second day, oocytes were injected with 25 nL of diluted cRNA (~0.03 ng/nL of $GluR1_i$ or ~0.001 ng/nL of a 1:1 mixture of NR1−1a and NR2A) and incubated in Barth's medium with gentamicin (50 μg/mL; G1397, Sigma, St. Louis, MO) at 17 °C. Oocytes were used for recordings from 3 to 6 days postinjection.

Two-Electrode Voltage Clamp Electrophysiology and Determination of Agonist EC_{50}. Recording of membrane currents in oocytes was performed by inserting two glass microelectrodes (resistance: 0.5−2.5 MΩ) filled with 3 M KCl into an oocyte emerged in frog Ringer's solution (in mM: 115 NaCl, 2 KCl, 1.8 $BaCl_2$, 5 HEPES, pH 7.6). Electrodes were voltage clamped with the use of a two-electrode voltage clamp amplifier (TEV-200A, Dagan Corporation, Minneapolis, MN). Recordings of membrane currents were made while the oocytes were continuously perfused with frog Ringer's solution. Drugs were dissolved in frog Ringer's solution and added to oocytes by full bath application. Agonist concentration−response relationships were constructed by measuring the maximal current induced by bath application of a saturating concentration of agonist to the oocyte (100 μM glutamate for GluR1; 100 μM glutamate and 100 μM glycine for NR1/NR2A), followed by application of compounds in increasing concentrations. The current responses (I) induced by application of a specific concentration of agonist was normalized to the response induced by saturating concentration of Glu (I_{GLU}). The mean of normalized responses from at least five oocytes were plotted as a function of agonist concentration. The concentration−response relationship was determined by curve-fitting of the four parameter logistic equation: $I/I_0 = 1/(1 + (EC_{50}/[\text{agonist}])^n)$, where I is the agonist-evoked current, I_0 is the agonist-evoked current in the absence of antagonist, [agonist] is the concentration of agonist, and n is the Hill slope.

The Fluo-4 Intracellular Calcium Imaging Assay. Stable $GluR1_i$, $GluR2(Q)_i$, $GluR3_i$, $GluR4_i$, GluR5(*Q*), and GluR6(*Q*) HEK293 cell lines were constructed and the functional properties of Glu and compounds **1** and **3**−**5** were characterized in the Fluo-4/AM assay as previously described.[30] The cells were split into poly-D-lysine-coated black 96-well plates with clear bottoms (BD Biosciences, Bedford, MA). After 16−24 h, the

medium was aspirated and the cells were incubated in 50 μL loading buffer (Hanks Buffered Saline Solution (HBSS) containing 20 mM HEPES, 1 mM $CaCl_2$, 1 mM $MgCl_2$ and 2.5 mM probenecid, pH 7.4) supplemented with 6 μM Fluo-4/AM (Molecular Probes, Eugene, OR) at 37 °C for 1 h. The loading buffer was aspirated, the cells were washed with 100 μL loading buffer, and then 100 μL assay buffer ((HBSS) containing 20 mM HEPES, 10 mM $CaCl_2$, 1 mM $MgCl_2$, and 2.5 mM probenecid, pH 7.4, supplemented with 100 μM CTZ in the case of GluR1−4 and with 1 mg/mL ConA in the case of GluR5−6) was added to the wells. Then the 96-well plate was assayed in a NOVOstar microplate reader (BMG Labtechnologies, Offenburg, Germany), measuring emission (in fluorescence units (FU)) at 520 nm caused by excitation at 485 nm before and up to 60 s after addition of 33 μL agonist solution (the agonists were dissolved in assay buffer). The experiments were performed in triplicate at least three times for each compound at each iGluR.

X-ray Structure Determination. Expression and crystallization of the GluR5-S1S2 construct comprising the ABD of GluR5 was achieved as previously described.[16] A protein solution of 4 mg/mL in 10 mM HEPES pH 7.0, 10 mM NaCl, 1 mM EDTA, and 10 mM **4** was used for crystallization with the hanging drop vapor diffusion method by mixing 1 μL of protein solution with 1 μL reservoir solution consisting of 18% PEG4000, 0.3 M Li_2SO_4, and 0.1 M Tris-HCl pH 7.5. Crystals grew within two days at 6 °C and were flash-frozen in liquid nitrogen after transfer through a cryoprotectant of 20% glycerol in reservoir solution. Data were collected at beamline ID14−1, ESRF, Grenoble, France, to 2.2 Å resolution and were processed using the HKL package.[43] The structure was solved by molecular replacement with the structure of GluR5-S1S2 in complex with domoic acid as template.[34] The program ARP/wARP[44] was used to automatically build 94% of the residues. Following manual rebuilding in program COOT,[45] the structure was refined with the program CNS[46] and the ligand could hereafter unambiguously be built into the electron density. The quality of the structure was validated using PROCHECK.[47] Domain openings were determined using DynDom.[48] Figure 3 was prepared in PyMOL.[49]

Computational Details. For the ligands **4** and **5** in solution, ab initio (LMP2/6-311+G**) and density functional theory (M06−2X/6-311+G**) optimizations including Poisson−Boltzmann self-consistent reaction field treatment of continuum solvation (PB-SCRF) were performed in *Jaguar 7.5*.[50] All atom models from both chains of GluR5-S1S2J:**4** as well as GluR2-S1S2J:**4** (PDB: 1WVJ) were prepared according to the standard protocol for bond assignment, hydrogen addition, H-bonding network optimization, and restrained minimization in *Maestro 8.5*.[49] QM-MM minimizations were performed in *Qsite 1.7*, which uses *Jaguar 7.5* and *Impact 5.0*.[49] The QM region consisted of the each ligand (**4**, (2*S*,8*R*)-**5**, and (2*S*,8*S*)-**5**) at M06−2X/6-311G** and the MM region was handled by the OPLS2005 forcefield, with constraints on all backbone atoms and side chains further than 6 Å from the ligand. Four input conformations each for **4**, (2*S*,8*R*)-**5**, and (2*S*,8*S*)-**5** were derived from conformational searches in *Macromodel 9.6*[49] in which the five fully or partially charged heteroatoms were constrained to the experimental positions and then least-squares superimposed with the native ligand in molA and molB. Hydrophobic and hydrophilic isopotentials were calculated on molA with the ligand, waters, and other heteroatoms removed, using *Sitemap 2.2*.[49] The enthalpies, entropies, and free energies of binding site water molecules with the ligand removed were calculated in *Watermap 1.0* within a 5 Å radius of the experimental positions of **4** in GluR2 (PDB: 1WVJ) and GluR5 (q.v., mol B) based on a pair of 9 ns molecular dynamics simulations in *Desmond 2.0*,[49,51] all with default settings, according to the method of Abel et al.[32,33] Figures depicting watermaps and site maps were produced in *Maestro 8.5*.[49]

Acknowledgment. The work was supported by grants from The Lundbeck Foundation, The Dansync Center for Synchrotron Radiation, The Drug Research Academy, and The Danish Medical Research Council. We thank people at ID14-1 and V. Soroka for data collection.

Supporting Information Available: Experimental procedures for synthesis of compounds **4**, **10a**, **11a**, **14a**, **17**, **19b**, **20a**, **20b**, **21a**, **21b**, **22a**, **22b**, **23a**, **23b**, **24a**, and **24b**. This material is available free of charge via the Internet at http://pubs.acs.org.

References

(1) Brauner-Osborne, H.; Egebjerg, J.; Nielsen, E. Ø.; Madsen, U.; Krogsgaard-Larsen, P. Ligands for glutamate receptors: design and therapeutic prospects. *J. Med. Chem.* **2000**, *43*, 2609–2645.
(2) Dingledine, R.; Borges, K.; Bowie, D.; Traynelis, S. F. The Glutamate Receptor Ion Channels. *Pharmacol. Rev.* **1999**, *51*, 7–62.
(3) Javitt, D. C. Glutamate as a therapeutic target in psychiatric disorders. *Mol. Psychiatry* **2004**, *9*, 984–997.
(4) Parsons, C. G.; Danysz, W.; Quack, G. Glutamate in CNS disorders as a target for drug development: an update. *Drug News Perspect.* **1998**, *11*, 523–569.
(5) James, N. C. K.; John, A. K. Ionotropic and metabotropic glutamate receptor structure and pharmacology. *Psychopharmacology* (*Berlin*) **2005**, 4–29.
(6) Erreger, K.; Chen, P. E.; Wyllie, D. J.; Traynelis, S. F. Glutamate receptor gating. *Crit Rev. Neurobiol.* **2004**, *16*, 187–224.
(7) Mayer, M. L. Glutamate receptor ion channels. *Curr. Opin. Neurobiol.* **2005**, *15*, 282–288.
(8) Mansour, M.; Nagarajan, N.; Nehring, R. B.; Clements, J. D.; Rosenmund, C. Heteromeric AMPA receptors assemble with a preferred subunit stoichiometry and spatial arrangement. *Neuron* **2001**, *32*, 841–853.
(9) Armstrong, N.; Sun, Y.; Chen, G. Q.; Gouaux, E. Structure of a glutamate−receptor ligand-binding core in complex with kainate. *Nature* **1998**, *395*, 913–917.
(10) Armstrong, N.; Gouaux, E. Mechanisms for activation and antagonism of an AMPA-sensitive glutamate receptor: crystal structures of the GluR2 ligand binding core. *Neuron* **2000**, *28*, 165–181.
(11) Hogner, A.; Kastrup, J.; Jin, R.; Liljefors, T.; Mayer, M.; Egebjerg, J.; Larsen, I.; Gouaux, E. Structural basis for AMPA receptor activation and ligand selectivity: crystal structures of five agonist complexes with the GluR2 ligand-binding core. *J. Mol. Biol.* **2002**, *322*, 93–109.
(12) Furukawa, H.; Gouaux, E. Mechanisms of activation, inhibition and specificity: crystal structures of the NMDA receptor NR1 ligand-binding core. *EMBO J.* **2003**, *22*, 2873–2885.
(13) Furukawa, H.; Singh, S. K.; Mancusso, R.; Gouaux, E. Subunit arrangement and function in NMDA receptors. *Nature* **2005**, *438*, 185–192.
(14) Mayer, M. L. Crystal structures of the GluR5 and GluR6 ligand binding cores: molecular mechanisms underlying kainate receptor selectivity. *Neuron* **2005**, *45*, 539–552.
(15) Nanao, M. H.; Green, T.; Stern-Bach, Y.; Heinemann, S. F.; Choe, S. Structure of the kainate receptor subunit GluR6 agonist-binding domain complexed with domoic acid. *Proc. Natl. Acad. Sci. U.S.A.* **2005**, *102*, 1708–1713.
(16) Naur, P.; Vestergaard, B.; Skov, L. K.; Egebjerg, J.; Gajhede, M.; Kastrup, J. S. Crystal structure of the kainate receptor GluR5 ligand-binding core in complex with (*S*)-glutamate. *FEBS Lett.* **2005**, *579*, 1154–1160.
(17) Naur, P.; Hansen, K. B.; Kristensen, A. S.; Dravid, S. M.; Pickering, D. S.; Olsen, L.; Vestergaard, B.; Egebjerg, J.; Gajhede, M.; Traynelis, S. F.; Kastrup, J. S. Ionotropic glutamate-like receptor delta 2 binds D-serine and glycine. *Proc. Natl. Acad. Sci. U.S.A.* **2007**, *104*, 14116–14121.
(18) Yao, Y.; Harrison, C. B.; Freddolino, P. L.; Schulten, K.; Mayer, M. L. Molecular mechanism of ligand recognition by NR3 subtype glutamate receptors. *EMBO J.* **2008**, *27*, 2158–2170.
(19) Yao, Y.; Mayer, M. L. Characterization of a soluble ligand binding domain of the NMDA receptor regulatory subunit NR3A. *J. Neurosci.* **2006**, *26*, 4559–4566.
(20) Ahmed, A. H.; Wang, Q.; Sondermann, H.; Oswald, R. E. Structure of the S1S2 glutamate binding domain of GLUR3. *Proteins* **2008**, *75*, 628–637.
(21) Kasper, C.; Frydenvang, K.; Naur, P.; Gajhede, M.; Pickering, D. S.; Kastrup, J. S. Molecular mechanism of agonist recognition by the ligand-binding core of the ionotropic glutamate receptor 4. *FEBS Lett.* **2008**, *582*, 4089–4094.

(22) Jin, R.; Banke, T. G.; Mayer, M. L.; Traynelis, S. F.; Gouaux, E. Structural basis for partial agonist action at ionotropic glutamate receptors. *Nat. Neurosci.* **2003**, *6*, 803–810.
(23) Frandsen, A.; Pickering, D. S.; Vestergaard, B.; Kasper, C.; Nielsen, B. B.; Greenwood, J. R.; Campiani, G.; Fattorusso, C.; Gajhede, M.; Schousboe, A.; Kastrup, J. S. Tyr702 is an important determinant of agonist binding and domain closure of the ligand-binding core of GluR2. *Mol. Pharmacol.* **2005**, *67*, 703–713.
(24) Brehm, L.; Greenwood, J. R.; Hansen, K. B.; Nielsen, B.; Egebjerg, J.; Stensbøl, T. B.; Brauner-Osborne, H.; Sløk, F. A.; Kronborg, T. T. A.; Krogsgaard-Larsen, P. (*S*)-2-Amino-3-(3-hydroxy-7,8-dihydro-6*H*-cyclohepta[*d*]isoxazol-4-yl)propionic acid, a potent and selective agonist at the GluR5 subtype of ionotropic glutamate receptors. Synthesis, modeling, and molecular pharmacology. *J. Med. Chem.* **2003**, *46*, 1350–1358.
(25) Krogsgaard-Larsen, P.; Nielsen, E. Q.; Curtis, D. R. Ibotenic acid analogs—synthesis and biological and in vitro activity of conformationally restricted agonists at central excitatory amino acid receptors. *J. Med. Chem.* **1984**, *27*, 585–591.
(26) Nielsen, B. B.; Pickering, D. S.; Greenwood, J. R.; Brehm, L.; Gajhede, M.; Schousboe, A.; Kastrup, J. S. Exploring the GluR2 ligand-binding core in complex with the bicyclical AMPA analogue (*S*)-4-AHCP. *FEBS J.* **2005**, *272*, 1639–1648.
(27) Borowitz, I. J.; Bandurco, V.; Beller, H.; Williams, G. J.; Suciu, N.; Gross, L.; Rigby, R. D. G.; Kurland, D. Medium ring compounds 0.7. Synthesis of 2-methyl-7-ketoundecanolide, 8-ketoundecanolide, and 2,4,6-trimethyl-7-ketodecanolide. *J. Org. Chem.* **1972**, *37*, 581–588.
(28) Jackson, R. F. W.; Moore, R. J.; Dexter, C. S.; Elliot, J.; Mowbray, C. E. Concise synthesis of enantiomerically pure phenylalanine, homophenylalanine, and bishomophenylalanine derivatives using organozinc chemistry: NMR studies of amino acid-derived organozinc reagents. *J. Org. Chem.* **1998**, *63*, 7875–7884.
(29) Siebum, A. H. G.; Woo, W. S.; Raap, J.; Lugtenburg, J. Access to any site-directed isotopomer of methionine, selenomethionine, cysteine, and selenocysteine—use of simple, efficient modular synthetic reaction schemes for isotope incorporation. *Eur. J. Org. Chem.* **2004**, 2905–2913.
(30) Strange, M.; Brauner-Osborne, H.; Jensen, A. A. Functional characterisation of homomeric ionotropic glutamate receptors GluR1-GluR6 in a fluorescence-based high throughput screening assay. *Comb. Chem. High Throughput Screening* **2006**, *9*, 147–158.
(31) Nielsen, M. M.; Liljefors, T.; Krogsgaard-Larsen, P.; Egebjerg, J. The Selective Activation of the Glutamate Receptor GluR5 by ATPA Is Controlled by Serine 741. *Mol. Pharmacol.* **2003**, *63*, 19–25.
(32) Abel, R.; Young, T.; Farid, R.; Berne, B. J.; Friesner, R. A. Role of the active-site solvent in the thermodynamics of factor Xa ligand binding. *J. Am. Chem. Soc.* **2008**, *130*, 2817–2831.
(33) Young, T.; Abel, R.; Kim, B.; Berne, B. J.; Friesner, R. A. Motifs for molecular recognition exploiting hydrophobic enclosure in protein−ligand binding. *Proc. Natl. Acad. Sci. U.S.A.* **2007**, *104*, 808–813.
(34) Hald, H.; Naur, P.; Pickering, D. S.; Sprogoe, D.; Madsen, U.; Timmermann, D. B.; Ahring, P. K.; Liljefors, T.; Schousboe, A.; Egebjerg, J.; Gajhede, M.; Kastrup, J. S. Partial agonism and antagonism of the ionotropic glutamate receptor iGluR5—Structures of the ligand-binding core in complex with domoic acid and 2-amino-3-[5-*tert*-butyl-3-(phosphonomethoxy)-4-isoxazolyl]propionic acid. *J. Biol. Chem.* **2007**, *282*, 25726–25736.
(35) Frandsen, A.; Pickering, D. S.; Vestergaard, B.; Kasper, C.; Nielsen, B. B.; Greenwood, J. R.; Campiani, G.; Fattorusso, C.; Gajhede, M.; Schousboe, A.; Kastrup, J. S. Tyr702 is an important determinant of agonist binding and domain closure of the ligand-binding core of GluR2. *Mol. Pharmacol.* **2005**, *67*, 703–713.
(36) Honore, T.; Nielsen, M. Complex structure of quisqualate-sensitive glutamate receptors in rat cortex. *Neurosci. Lett.* **1985**, *54*, 27–32.
(37) Braitman, D. J.; Coyle, J. T. Inhibition of [^{3}H]kainic acid receptor binding by divalent cations correlates with ion affinity for the calcium channel. *Neuropharmacology* **1987**, *26*, 1247–1251.
(38) Sills, M. A.; Fagg, D.; Pozza, M.; Angst, C.; Brundish, D. E.; Hurt, S. D.; Wilusz, E. J.; Williams, M. [^{3}H]CGP 39653: a new *N*-methyl-D-aspartate antagonist radioligand with low nanomolar affnity in rat brain. *Eur. J. Pharmacol.* **1991**, *192*, 19–24.
(39) Hermit, M. B.; Greenwood, J. R.; Nielsen, B.; Bunch, L.; Jørgensen, C. G.; Vestergaard, H. T.; Stensbøl, T. B.; Sanchez, C.; Krogsgaard-Larsen, P.; Madsen, U.; Brauner-Osborne, H. Ibotenic acid and thioibotenic acid: a remarkable difference in activity at group III metabotropic glutamate receptors. *Eur. J. Pharmacol.* **2004**, *486*, 241–250.
(40) Ransom, R. W.; Stec, N. L. Cooperative modulation of [^{3}H]MK801 binding to the *N*-methyl-D-aspartate receptor ion channel complex by L-glutamate, glycine and polyamines. *J. Neurochem.* **1988**, *51*, 830–836.
(41) Vogensen, S. B.; Clausen, R. P.; Greenwood, J. R.; Johansen, T. N.; Pickering, D. S.; Nielsen, B.; Ebert, B.; Krogsgaard-Larsen, P. Convergent synthesis and pharmacology of substituted tetrazolyl-2-amino-3-(3-hydroxy-5-methyl-4-isoxazolyl)propionic acid analogues. *J. Med. Chem.* **2005**, *48*, 3438–3442.
(42) Sagot, E.; Pickering, D. S.; Pu, X.; Umberti, M.; Stensbol, T. B.; Nielsen, B.; Chapelet, M.; Bolte, J.; Gefflaut, T.; Bunch, L. Chemoenzymatic synthesis of a series of 2,4-*syn*-functionalized (*S*)-glutamate analogues: new insight into the structure−activity relation of ionotropic glutamate receptor subtypes 5, 6, and 7. *J. Med. Chem.* **2008**, *51*, 4093–4103.
(43) Otwinowski, Z.; Minor, W. Processing of X-ray diffraction data collected in oscillation mode. *Macromol. Crystallogr., Part A* **1997**, *276*, 307–326.
(44) Perrakis, A.; Morris, R.; Lamzin, V. S. Automated protein model building combined with iterative structure refinement. *Nat. Struct. Biol.* **1999**, *6*, 458–463.
(45) Emsley, P.; Cowtan, K. Coot: model-building tools for molecular graphics. *Acta Crystallogr., Sect D: Biol. Crystallogr.* **2004**, *60*, 2126–2132.
(46) Brunger, A. T.; Adams, P. D.; Clore, G. M.; Delano, W. L.; Gros, P.; Grosse-Kunstleve, R. W.; Jiang, J. S.; Kuszewski, J.; Nilges, M.; Pannu, N. S.; Read, R. J.; Rice, L. M.; Simonson, T.; Warren, G. L. Crystallography & NMR system: a new software suite for macromolecular structure determination. *Acta Crystallogr., Sect D: Biol. Crystallogr.* **1998**, *54*, 905–921.
(47) Laskowski, R. A.; Macarthur, M. W.; Moss, D. S.; Thornton, J. M. Procheck—A Program to Check the Stereochemical Quality of Protein Structures. *J. Appl. Crystallogr.* **1993**, *26*, 283–291.
(48) Hayward, S.; Lee, R. A. Improvements in the analysis of domain motions in proteins from conformational change: DynDom version 1.50. *J. Mol. Graph. Model.* **2002**, *21*, 181–183.
(49) Delano, W. L. *The PyMOL Molecular Graphics System*; Delano Scientific: San Carlos, CA, 2002.
(50) *Schrodinger Suite 2008*; Schrodinger LLC: 101 SW Main Street, Suite 1300, Portland, OR 97204, 2008.
(51) *Desmond 2.0*; D. E. Shaw Research LLC: 120 West 45th Street, 39th Floor, New York, NY 10036, 2008.
(52) Vogensen, S. B.; Greenwood, J. R.; Varming, A. R.; Brehm, L.; Pickering, D. S.; Nielsen, B.; Liljefors, T.; Clausen, R. P.; Johansen, T. N.; Krogsgaard-Larsen, P. A stereochemical anomaly: the cyclised (*R*)-AMPA analogue (*R*)-3-hydroxy-4,5,6,7-tetrahydroisoxazolo[5,4-*c*]pyridine-5-carboxylic acid [(*R*)-5-HPCA] resembles (*S*)-AMPA at glutamate receptors. *Org. Biomol. Chem.* **2004**, *2*, 206–213.
(53) Stensbøl, T. B.; Borre, L.; Johansen, T. N.; Egebjerg, J.; Madsen, U.; Ebert, B.; Krogsgaard-Larsen, P. Resolution, absolute stereochemistry and molecular pharmacology of the enantiomers of ATPA. *Eur. J. Pharmacol.* **1999**, *380*, 153–162.
(54) Kleywegt, G. J.; Jones, T. A. Phi/psi-chology: Ramachandran revisited. *Structure* **1996**, *4*, 1395–1400.